

Magnetar giant flare oscillations and the nuclear symmetry energy

Alex T. Deibel *

*Department of Physics and Astronomy, Michigan State University, East Lansing, MI 48824, USA and
The Joint Institute for Nuclear Astrophysics*

Andrew W. Steiner

*The Joint Institute for Nuclear Astrophysics and
Institute for Nuclear Theory, University of Washington, Seattle, WA 98195, USA*

Edward F. Brown

*Department of Physics and Astronomy, Michigan State University, East Lansing, MI 48824, USA,
The Joint Institute for Nuclear Astrophysics and
National Superconducting Cyclotron Laboratory, Michigan State University, East Lansing, MI 48824, USA*

If the observed quasi-periodic oscillations in magnetar flares are partially confined to the crust, then the oscillation frequencies are unique probes of the nuclear physics of the neutron star crust. We study crustal oscillations in magnetars including corrections for a finite Alfvén velocity. Our crust model uses a new nuclear mass formula that predicts nuclear masses with an accuracy very close to that of the finite range droplet model. This mass model for equilibrium nuclei also includes shell corrections and an updated neutron-drip line. We perturb our crust model to predict axial crust modes and assign them to observed giant flare quasi-periodic oscillation frequencies from the soft γ -ray repeater SGR 1806-20. We find magnetar crusts that match observations for various magnetic field strengths, entrainment of the free neutron gas in the inner crust, and crust-core transition densities. We find that observations can be reconciled with smaller values of the symmetry energy slope parameter, L , if there is a significant amount of entrainment of the neutrons by the superfluid or if the crust-core transition density is large. We also find neutron star masses and radii which are in agreement with expectations from what is known about low-density matter from nuclear experiment. Matching observations with a field-free model we obtain the approximate values of $M = 1.35 M_{\odot}$ and $R = 11.9$ km. Matching observations using a model with the surface dipole field of SGR 1806-20 ($B = 2.4 \times 10^{15}$ G) we obtain the approximate values of $M = 1.25 M_{\odot}$ and $R = 12.4$ km.

PACS numbers: 97.60.Jd 21.65.Mn 26.60.Gj

I. INTRODUCTION

Highly magnetized and isolated neutron stars, known as magnetars, emit irregular and extremely energetic γ -ray flares. These flares are thought to occur following a starquake, in which a reconfiguration of the magnetic field fractures the magnetar's crust. Quasi-periodic oscillations (QPOs) are observed in the tails of giant flare emissions [1–4]. Following the proposal by Duncan [5], many have attempted to model the QPOs as torsional modes of the crust [e.g., 6–8]. If this is indeed the cause of the QPOs, then magnetars can give a unique insight into the microphysics of the neutron star crust [9], e.g., the nuclear symmetry energy $S(n)$, here defined as the difference in energy between pure neutron matter and proton-neutron symmetric matter as a function of the baryon density, n . In particular, crust frequencies are sensitive to the quantity $L \equiv 3n_0 (\partial S / \partial n)_{n=n_0}$ [9, 10]. In addition, different modes have different scalings with the neutron star mass and radius; it follows that observations of two or more modes, such as a fundamental and harmonic, can constrain the magnetar's mass and radius [8, 11] and hence the equation of state (EOS) of dense matter.

In this paper, we explore the impact on constraints of the symmetry energy and the properties of the crust under the assumption that one of the lower frequency QPOs and a higher frequency QPO, such as the 626 Hz mode observed from the soft γ -ray repeater SGR 1806-20 [4], represent the fundamental and first harmonic modes of the crust. Our study extends previous work by using a modern EOS to predict torsional mode frequencies and by matching observations for various magnetic field strengths, entrainment fractions for free neutrons in the inner crust, and crust-core transition densities. The crust EOS is based on a liquid droplet model which predicts nuclear masses to within 1.2 MeV [12], close to the accuracy obtained in the finite range droplet model [13]. By adding the effect of the magnetic field on electrons, as in Broderick et al. [14], we revise the magnetic composition of the crust [15] with a new determination of equilibrium nuclei. The core EOS is based on recent neutron star mass and radius constraints from observations of photosphere radius expansion bursts (PREs) and the quiescent emission of low-mass x-ray binaries (LMXBs) [16, 17].

While this initial study incorporates a modern EOS, it necessarily makes many simplifying assumptions. The basis of our approach is the assumption that the QPOs in question are indeed due to torsional crust modes. An alternative model associates the QPOs with magnetohydrodynamic (MHD) modes in the core [18, 19]. We note that neither model is able to predict all of the observed mode frequencies. Crustal oscilla-

*deibelal@msu.edu

tions cannot easily reproduce all of the low-frequency modes [8]. Recent studies of core MHD modes with crust-core coupling in a dipolar magnetic field found that core MHD modes could explain most of the QPOs, but only with a magnetic field larger than the observed surface dipole fields [20]. In addition, core MHD models have been unable to reproduce the highest QPO frequencies observed [21]. Stratification and entrainment can increase core MHD frequencies, but this does not yet completely explain the data either [22]. We also do not include a consistent treatment of the nuclear pasta or its shear viscosity. We comment on how this might modify our results at the end.

With these caveats, we construct magnetized crust models for equations of state with extreme values of L , free neutron entrainment, crust-core transition densities, and different high-density equations of state. In Sec. II we present the magnetized crust composition based on our mass model (a detailed description of this formalism is in Appendix A). Section III contains a summary of the axial perturbation equations for the crust modes. We then use, in Sec. IV, the predicted fundamental and harmonic frequencies, along with the magnetized crust composition, to investigate the role of the nuclear symmetry energy in determining magnetar masses, radii, and crust oscillation frequencies. In Sec. V, we discuss our results.

II. CRUST COMPOSITION

For an isolated neutron star we determine the crust composition by finding the ground-state nucleus at a given baryon density n . The outer crust consists of a lattice of nuclei embedded in a degenerate electron Fermi gas [23]. The neutron-drip point, the point at which it becomes energetically favorable for neutrons to exist outside of the nuclei, defines the boundary between the outer and inner crust. The inner crust can then be described as a lattice of nuclei embedded in both an electron and neutron gas [23]. We use a liquid droplet model with “squared-off” nuclear density distributions [24] and assume that the number density of neutrons and protons inside nuclei is fixed and that the number density of neutrons outside nuclei is fixed in a way as to obtain equilibrium. The nuclei occupy a fraction, χ , of the total volume of a Wigner-Seitz cell and the dripped neutrons in the inner crust occupy a fraction, $1 - \chi$, of the total volume. This separation of the neutron gas from the nuclei is convenient for modeling the properties of matter at high densities [12]. As described in Appendix A, at a given n , proton number Z , and atomic number A , the total energy density of the crust will have contributions from the nuclear binding energy, the Coulomb lattice, the electron gas, and the neutron gas. Both the bulk energy of the nucleus and the energy of the neutron gas are determined by the same Skyrme interaction, either SLy4 with $L = 46$ MeV or Rs with $L = 86$ MeV. The liquid drop model parameters [12] are fit to experimental nuclear masses separately for each interaction. The fits for each interaction differ because the value of L determines the surface energy and surface symmetry energy parameters. Both models give similar quality fits to the data. Chamel et al. [25] obtained qualitatively similar results using

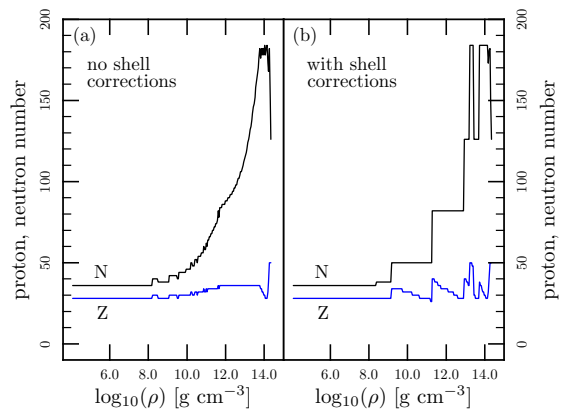


FIG. 1: (Color online) Equilibrium composition of the crust without a magnetic field for (a) a model that neglects shell effects and (b) a model that includes them. The blue lower curve corresponds to the proton number Z and the black upper curve corresponds to the neutron number N .

Hartree-Fock-Bogoliubov models.

At a given n the equilibrium nucleus minimizes the total energy density of the system. The most energetically favorable nuclei tend to contain a closed shell of protons or neutrons due to shell corrections [26, 27]. As n increases, equilibrium nuclei will move to higher closed shells of protons and neutrons with the most neutron-rich nuclei seen between the neutron-drip point and the crust-core transition. The above features of the crust composition can be seen in Fig. 1. We ignore the deformation of nuclei at high densities in the crust composition.

In the outer crust a strong magnetic field will force electrons to occupy the lowest Landau levels. At higher baryon densities electrons can occupy higher Landau levels and thus their energy density approaches the field-free case. For this reason, as seen in Table I, only the outer crust equilibrium composition is significantly altered. For $B < 10^{18}$ G we can ignore both the effect of the magnetic field on the structure of the nuclei in the crust [see, e.g., 28, 29] and on the gross structure of the neutron star [30].

III. TORSIONAL OSCILLATIONS IN A STRONG MAGNETIC FIELD

We describe the axial crust modes of an oscillating neutron star in the relativistic Cowling approximation following the work of Schumaker and Thorne [31] and Samuelsson and Andersson [8]. We combine two forms of the axial perturbation equation. In the non-magnetic case, the equation for the axial perturbation ξ can be written in the form [8] $\xi'' + F'\xi' + G\xi = 0$, in which primes indicate derivatives with respect to the radial coordinate, and F and G are functions of the shear velocity v_s and the metric functions ν and λ for a static and spherically symmetric space-time metric, $ds^2 = -e^{2\nu} dt^2 + e^{2\lambda} dr^2 + r^2 (d\theta^2 + \sin^2 \theta d\phi^2)$. Because of the strong vertical stratification, radial perturbations are driven to small amplitudes and high frequencies and are much less rel-

TABLE I: Magnetic Equilibrium Nuclei Below Crust-Core Transition

| Nuclei ^a | ρ_{\max} (g cm ⁻³) | | | | |
|---------------------------------|-------------------------------------|-----------|--------------------|-----------------------|-----------------------|
| | $B_* = 0$ | $B_* = 1$ | $B_* = 10$ | $B_* = 10^2$ | $B_* = 10^3$ |
| ⁶⁴ ₂₈ Ni | 2.23×10^8 | | 2.33×10^8 | 1.63×10^9 | 1.75×10^{10} |
| ⁶⁶ ₂₈ Ni | 1.37×10^9 | | 1.40×10^9 | 2.92×10^9 | 2.71×10^{10} |
| ⁸⁴ ₃₄ Se | 5.66×10^9 | | | 4.87×10^9 | 5.29×10^{10} |
| ⁸² ₃₂ Ge | 1.73×10^{10} | | | 1.69×10^{10} | 7.62×10^{10} |
| ⁸⁰ ₃₀ Zn | 3.99×10^{10} | | | 3.94×10^{10} | 1.01×10^{11} |
| ⁷⁸ ₂₈ Ni | 1.56×10^{11} | | | 1.57×10^{11} | 1.61×10^{11} |
| ⁷⁶ ₂₆ Fe | 1.86×10^{11} | | | 1.85×10^{11} | 1.76×10^{11} |
| ¹²² ₄₀ Zr | 2.51×10^{11} | | | 2.52×10^{11} | 1.98×10^{11} |
| ¹²⁰ ₃₈ Sr | 3.54×10^{11} | | | 3.54×10^{11} | 4.04×10^{11} |
| ¹¹⁸ ₃₆ Kr | 5.17×10^{11} | | | 5.15×10^{11} | 5.77×10^{11} |
| ¹¹⁶ ₃₄ Se | 8.11×10^{11} | | | 8.13×10^{11} | 8.56×10^{11} |
| ¹¹⁴ ₃₂ Ge | 2.35×10^{12} | | | | 2.25×10^{12} |
| ¹¹² ₃₀ Zn | 3.94×10^{12} | | | | 4.02×10^{12} |
| ¹¹⁰ ₂₈ Ni | 8.64×10^{12} | | | | 8.65×10^{12} |
| ¹⁶⁶ ₄₀ Zr | 1.07×10^{13} | | | | 1.08×10^{13} |

^aWe adopt the format of Lai and Shapiro [15] where ρ_{\max} is the maximum mass density where the equilibrium nucleus is present. If a density value is unchanged the following column is blank. Here $B_* = B/(4.414 \times 10^{13} \text{ G})$, which is the ratio of the magnetic field to the critical field, defined as the field at which the cyclotron energy equals the electron rest-mass.

evant in the crust. Working in the isotropic limit, we incorporate corrections for a finite Alfvén velocity $v_A = B/\sqrt{4\pi\rho_i}$ in the radial direction by analogy with the Newtonian expressions [6, 9]. A more complicated magnetic field configuration is worthy of study, but we find below that crustal frequencies are more sensitive to entrainment and the EOS and thus we choose a uniform magnetic field for now. The result is

$$\begin{aligned} (v_s^2 + v_A^2)\xi'' + v_s^2 \frac{d}{dr} \left\{ \ln \left[r^4 e^{v-\lambda} (\varepsilon + p) v_s^2 \right] \right\} \xi' \\ + e^{2\lambda} \left[e^{-2\nu} \omega^2 \left(1 + \frac{v_A^2}{c^2} \right) - \frac{(l^2 + l - 2)v_s^2}{r^2} \right] \xi = 0. \end{aligned} \quad (1)$$

In this expression r is the radius, ε is the energy density, p is the pressure, ω is the angular frequency, and l is the angular wave number. The shear velocity is $v_s = \sqrt{\mu/\rho}$, which is plotted with the Alfvén velocity in Fig. 2. Here μ is the shear modulus, for which we use the formulation appropriate for a body-centered cubic lattice [32],

$$\mu = \frac{0.1194\Gamma}{1 + 0.595(\Gamma_0/\Gamma)^2} n_i k_B T. \quad (2)$$

We integrate Equation (1) over the solid crust, which lies between the crust-core interface at $r = R_{\text{core}}$ and where the lattice melts at $r = R_{\text{crust}}$. The melting transition is determined by where the plasma coupling parameter $\Gamma = (Ze)^2/ak_B T = \Gamma_{\text{melt}} = 175$ [33, 34]. Here $a = (3/4\pi n_i)^{1/3}$ is the radius of the

Wigner-Seitz cell, Z is the atomic charge number, n_i is the ion number density, and the temperature is $T = 3.0 \times 10^8 \text{ K}$.

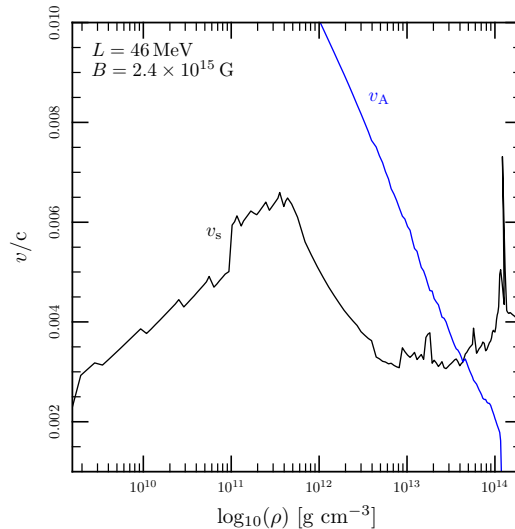


FIG. 2: (Color online) Alfvén velocity (blue curve) and shear velocity (black curve) in the crust as a function of mass density. The composition is that of a $1.4 M_\odot$ neutron star using the SLy4 crust EOS.

For the boundary conditions needed to solve Equation (1),

we require the traction, ξ' , to vanish at the top and bottom of the crust. This is a good approximation near the surface where pressure vanishes. The description of matter near the crust-core transition is complicated by the appearance of nuclear pasta. Since the quasi-free neutrons are superfluid, assuming the traction vanishes at the crust-core boundary may also be a good approximation. An additional impact of the superfluid is that some fraction, f_{ent} , of the quasi-free neutrons are entrained with the nuclei [35, 36]. We assume zero traction at the crust-core transition and leave a more complete description of matter at the highest densities to future work.

For a given l , Equation (1), when integrated over the crust with the boundary conditions described here, has an eigenvalue ω that is uniquely determined by the crust thickness $\Delta = R_{\text{crust}} - R_{\text{core}}$ and the neutron star radius. These in turn depend on the equation of state.

IV. THE NUCLEAR PHYSICS OF THE CRUST

QPO frequencies have been detected in two magnetars, SGR 1806–20 and SGR 1900+14 [2–4, 7]. The 29 Hz mode in SGR 1806–20 and the 28 Hz mode in SGR 1900+14 are often assumed to be the fundamental torsional modes, but an 18 Hz mode was also observed in SGR 1806–20 and a lower frequency mode is not ruled out by the 1900+14 data. SGR 1806–20 also showed a very clear 626 Hz mode, possibly matching the first radial harmonic ($n = 1$). Several other modes are observed between 50 and 200 Hz, and these can be matched with higher angular momentum harmonics, $l > 1$. However, the frequency spacing is small between the $l > 1$ harmonics and this makes matching observed modes to particular angular momentum harmonics ambiguous. We exclude an analysis of the higher angular momentum harmonics because they do not lead to superior mass and radius constraints.

A. The equation of state

For the core, we use the probability distribution for the EOS determined by Steiner et al. [17] from observations of PREs and from the quiescent emission of LMXBs. We construct five equations of state corresponding to the most probable mass-radius relation along with its 1- and 2- σ lower and upper bounds. Our core model is distinct from the interaction used to describe matter in the crust (Skyrme models SLy4 or Rs) because we wish to avoid the additional assumption that the physics of matter at low and high densities is correlated. If we were to use the SLy4 EOS in the core, the radius of a $1.4 M_{\odot}$ neutron star is 11.65 km [37], a bit larger than the lower 1- σ results from Steiner et al. [17]. For the Rs EOS, the radius of a $1.4 M_{\odot}$ neutron star is 13.04 km, which is very similar to the largest radius implied by the mass and radius observations from Steiner et al. [17]. Each equation of state gives mass-radius combinations with different crust thicknesses, and hence a unique fundamental mode ($n = 0$) and harmonic mode ($n = 1$). We can constrain the masses and radii of magnetars by matching predicted fundamental modes

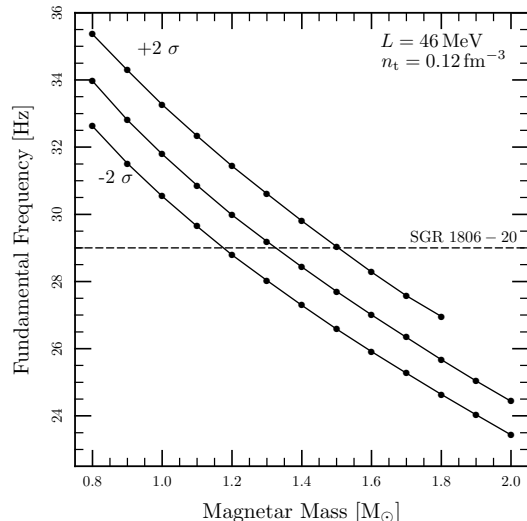


FIG. 3: Frequency of the fundamental $l = 2$ mode as a function of the magnetar mass for the core EOS probability distribution (centroid and $\pm 2\sigma$) from Steiner et al. [17] and an SLy4 crust EOS. The dashed black line indicates the observed 29 Hz QPO of SGR 1806–20. The frequencies are evaluated for a crust-core transition density of 0.12 fm^{-3} with $B = 0 \text{ G}$.

and harmonic modes to observed QPOs. While general relativistic corrections tend to decrease the frequencies, softer core equations of state with smaller radii tend to increase the frequencies. Because of this latter effect, we get frequencies which are larger than that obtained by Steiner and Watts [9]. The $n = 0$, $l = 2$ mode corresponds to the 29 Hz QPO of SGR 1806–20. Our model predicts $n = 1$ harmonic modes near 600 Hz and we compare these predicted modes with the 626 Hz QPO of SGR 1806–20.

To find crusts with fundamentals that match the 29 Hz QPO we model crust perturbations in magnetars between $0.8\text{--}2.0 M_{\odot}$ with magnetic fields matching the surface dipole field of SGR 1806–20. Whichever crust has an $n = 0$, $l = 2$ mode that matches the 29 Hz QPO we take as the crust of the magnetar. This method is demonstrated in Fig. 3 where crusts are constructed using the SLy4 crust EOS [38]. Crusts with harmonics that match the 626 Hz QPO are found using an identical technique. We take whichever crust has an $n = 1$ mode that reproduces the observed QPO as the crust of the magnetar. The same analysis is repeated for the 1 and 2- σ lower and upper bounds on the core EOS.

A comparison of masses and radii from fundamental and harmonic modes can be seen in Fig. 4. The intersection of fundamental and harmonic masses and radii on the mass versus radius plot gives a crust that best matches the properties of SGR 1806–20. The mass and radius found for SGR 1806–20 depend on the properties of the interior of the magnetar which determine the fundamental and harmonic modes. This study focuses on varying three aspects of the interior physics that remain unknown, namely, the magnetic field strength in the crust, the crust-core transition density, and the degree of free neutron entrainment in the inner crust.

Different equations of state have different values of L and thus different fundamental mode frequencies. The SLy4 EOS has a 29 Hz $n = 0, l = 2$ fundamental mode. The Rs EOS gives frequencies between 15–20 Hz for the $n = 0, l = 2$ fundamental mode. Therefore, we must assign the predicted fundamental modes from Rs to the observed 18 Hz QPO. The Rs model has a smaller fundamental frequency than SLy4 because its symmetry energy increases more rapidly with density than does that of SLy4. With the density dependence of the nuclear symmetry energy defined as $L \equiv 3n_0 (\partial S / \partial n)_{n=n_0}$, the Rs model has $L = 86$ MeV at $n_0 = 0.16$ fm $^{-3}$, the nuclear saturation density, whereas the SLy4 model has $L = 46$ MeV. The shear modulus is proportional to the plasma coupling parameter Γ , which goes as Z^2/a (see Equation (2)). A larger value of L tends to increase the nucleon number A , which leads to larger a ; the charge number Z is almost unchanged, however, due to nuclear shell effects. Thus a larger value of L decreases the shear modulus and also the fundamental QPO frequency [9, 10].

B. The crust magnetic field

We examine the sensitivity of fundamental and harmonic modes to the strength of the magnetic field. Strong magnetic fields melt the outermost boundary of the crust (i.e., push the melting point of the one-component plasma to higher pressures). Since R_{core} remains fixed and R_{crust} decreases, a strong magnetic field thins the crust (i.e., decreases Δ). Although a strong magnetic field can decrease the crust thickness and change the composition of the outer crust, the overall impact on predicted fundamental and harmonic mode frequencies is negligible. We find that predicted fundamental modes from magnetized crusts are nearly identical to the field-free case, in agreement with the findings by Nandi et al. [39]. The magnetic field is not a determining factor because fundamental crust modes are entirely set by our choice of radius for the magnetar. That is, fundamental modes are entirely set by the equation of state. However, a magnetized crust can significantly alter predicted harmonic modes. The $n = 1$ modes are sensitive to the magnetic field, especially in the outer crust where $v_A > v_s$ [6, 39]. For example, to obtain a mass-radius solution consistent with the findings of Steiner et al. [17] for the Rs EOS requires $B \lesssim 10^{15}$ G. The magnetized crusts that match observed QPOs can be seen in Fig. 4.

C. The crust-core transition density

We test two extreme values for the crust-core transition density, n_t , from Oyamatsu and Iida [40]. The exact value of the crust-core transition density is unknown, in part because the density dependence of the nuclear symmetry energy in the inner crust is not well constrained and also because of the possible existence of nuclear pasta [see, e.g., 41]. Although previous works have found correlations between n_t and L [41], these correlations are still rather model-dependent. In Fig. 4, we examine various magnetic field strengths to

find masses and radii from intersections of fundamentals and harmonics for each transition density. For the SLy4 EOS, $n_t = 0.12$ fm $^{-3}$, and a surface dipole field matching that of SGR 1806-20 [42] ($B = 2.4 \times 10^{15}$ G) we find the magnetar to have $M = 1.25 M_\odot$ and $R = 12.4$ km. We must extrapolate outside the equation of state curves to approximate a mass and radius for the lower crust-core transition density $n_t = 0.08$ fm $^{-3}$, as can be seen in Fig. 5. This crust-core transition gives $M = 0.96 M_\odot$ and $R = 13.5$ km for SGR 1806-20. In either case, if we assume that the magnetic field inside the crust is larger than the observed surface field, then a smaller mass and larger radius is implied. If the magnetic field is too large, the implied radius will be far outside the radii implied by mass and radius observations from the quiescent LMXBs in M13 and ω Cen [16]. Using the Rs EOS, $n_t = 0.12$ fm $^{-3}$, and a surface dipole field matching that of SGR 1806-20 ($B = 2.4 \times 10^{15}$ G) we find the magnetar to have $M = 1.10 M_\odot$ and $R = 13.8$ km, which is outside the $2\text{-}\sigma$ mass-radius relation of Steiner et al. [17], as can be seen in Fig. 4.

Figure 4 also demonstrates that only harmonic modes are affected by a change in the crust-core transition density. A change in the crust-core transition density will change the crust thickness and harmonic modes scale with the crust thickness. Fundamental modes remain unchanged, however, because they scale with the radius of the entire star.

D. The entrainment of the free neutron gas

Entrainment of the free neutron gas in the inner crust alters both fundamental and harmonic modes, as shown in Fig. 6. We define the degree of entrainment f_{ent} as the fraction of the free neutron gas that moves with the lattice during a crust oscillation. Although f_{ent} only slightly alters the harmonic frequency, mainly by changing v_s , it significantly alters the fundamental mode frequency. This occurs because the fundamental mode energy is concentrated deeper in the crust, whereas harmonic modes have their energy distributed more uniformly over the crust [6]. If a lower fraction of the free neutrons are entrained, then larger masses and radii are implied for the magnetar. We find that a large degree of entrainment, $f_{\text{ent}} > 0.75$, is required for predicted crust modes to match observed QPOs using crust models built upon the SLy4 interaction [38]. As shown in Fig. 7, for the Rs EOS the predicted $n = 0, l = 2$ fundamental gives frequencies near the 29 Hz QPO of SGR 1806-20 when there is a low degree of entrainment of the free neutrons. For example, for $f_{\text{ent}} = 0.25$ we find the magnetar to have $M = 1.12 M_\odot$ and $R = 12.0$ km.

V. DISCUSSION

Magnetar giant flare QPOs provide a unique opportunity to probe the nuclear physics of the neutron star crust. Fundamental torsional modes are largely independent of the crust-core transition density and the magnetic field strength. Harmonic modes are sensitive to the surface gravity, transition

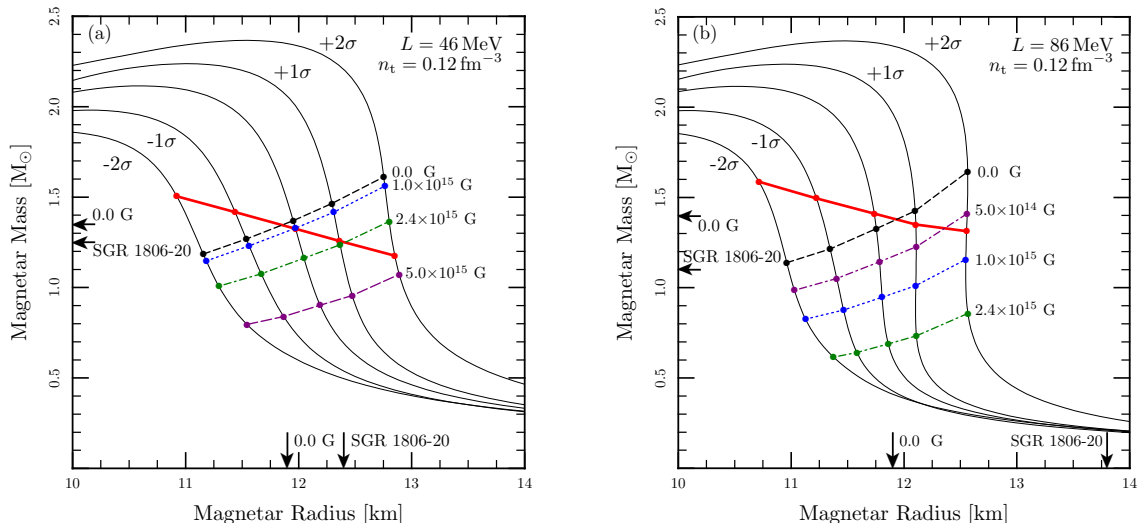


FIG. 4: (Color online) Magnetar mass as a function of radius for the core EOS probability distribution from Steiner et al. [17]. Frequencies are evaluated using (a) the SLy4 crust EOS ($L = 46$ MeV) and (b) the Rs crust EOS ($L = 86$ MeV), both for $n_t = 0.12$ fm $^{-3}$. The thick red solid line indicates masses and radii for which the fundamental mode has a frequency of 29 Hz in the case of SLy4 and 18 Hz in the case of Rs. The black short-dashed line indicates masses and radii for a 626 Hz harmonic mode and $B = 0$ G. Masses and radii from 626 Hz harmonic modes with magnetized crusts are labeled accordingly. Arrows indicate masses and radii that match both the fundamental and the harmonic modes for the field-free case and the case with the magnetic field of SGR 1806-20 ($B = 2.4 \times 10^{15}$ G).

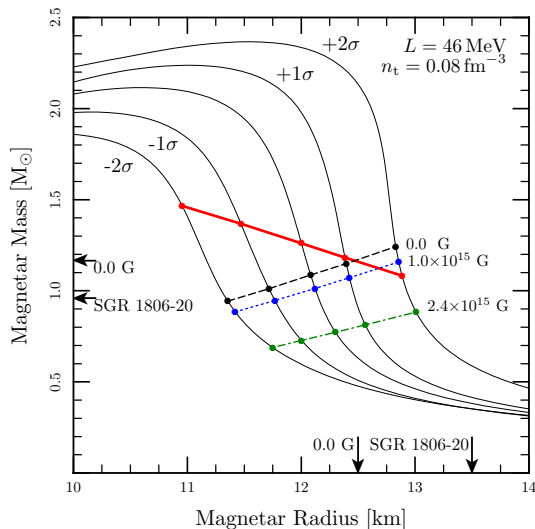


FIG. 5: (Color online) Same as Fig. 4, but for the SLy4 crust EOS with $n_t = 0.08$ fm $^{-3}$. The thick red solid line indicates masses and radii determined from a fundamental mode of 29 Hz. Masses and radii from harmonic modes with magnetized crusts are labeled accordingly. Arrows indicate masses and radii that match both the fundamental and the harmonic modes for the field-free case and the case with the magnetic field of SGR 1806-20 ($B = 2.4 \times 10^{15}$ G).

density, entrapment of the free neutrons, and the magnetic field strength. Comparison of fundamental and harmonic modes gives solutions for magnetar masses and radii and hence places constraints on L . In particular, we find values

of L that give results consistent with observed oscillations. For the SLy4 EOS, solutions most consistent with these constraints have large crust-core transition densities and a large degree of free neutron entrapment; those for the Rs EOS have large crust-core transition densities and a small degree of free neutron entrapment.

We find, in agreement with Sotani et al. [10], smaller fundamental mode frequencies for crust equations of state with larger values of L . Both works find that more entrapment decreases the fundamental frequency (in the notation of Sotani et al. [10], $N_s/N_d = 1 - f_{\text{ent}}$). Our work includes nuclear shell effects in a more consistent fashion, and thus it is more difficult to vary L continuously as in Sotani et al. [10]. Also, we only employ equations of state that are consistent with recent constraints from neutron star mass and radius measurements [17] that rule out larger values of L . A complete evaluation of how the entrapment in the crust might be correlated with L is needed and work in this direction is in progress.

Although fundamental modes are only slightly affected by the crust-core transition density, a larger transition density increases the crust thickness, for a fixed mass and radius, and drives the harmonic frequency lower. To match the observed harmonic with a larger transition density therefore requires a larger mass for a fixed radius.

The degree of entrapment of the free neutron gas in the inner crust alters both fundamental and harmonic modes by changing the shear velocity [35]. The fundamental mode is most sensitive to the entrapment fraction at the highest densities in the crust. A recent study of neutron entrapment via Bragg scattering with the crystal lattice gives $f_{\text{ent}} \approx 0.35$ – 0.90 throughout the inner crust [35]. Since the density dependence of neutron entrapment is model dependent and has not been

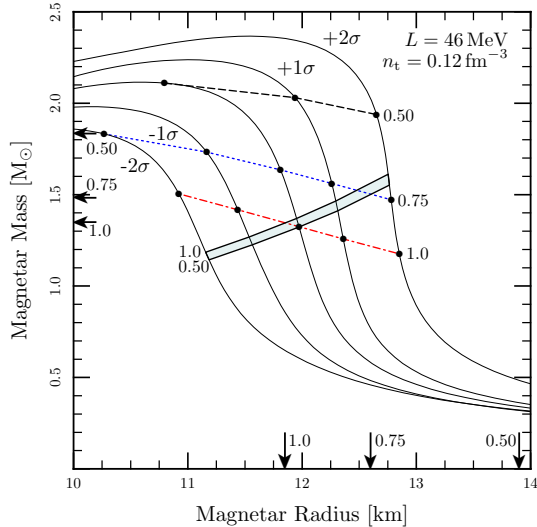


FIG. 6: (Color online) Magnetar mass as a function of radius for the core EOS probability distribution from Steiner et al. [17]. Frequencies are evaluated using the SLy4 crust EOS with $B = 0$ G and $n_t = 0.12 \text{ fm}^{-3}$. The red dot-dashed, blue dotted, and black dashed lines indicate masses and radii from fundamental modes of frequency 29 Hz for different free neutron entrainment fractions f_{ent} . The shaded band indicates masses and radii from 626 Hz harmonic modes as f_{ent} is varied from 0.50 to 1.0. Arrows indicate the masses and radii that match both the fundamental and the harmonic modes for $f_{\text{ent}} = 1.0, 0.75,$ and 0.50 .

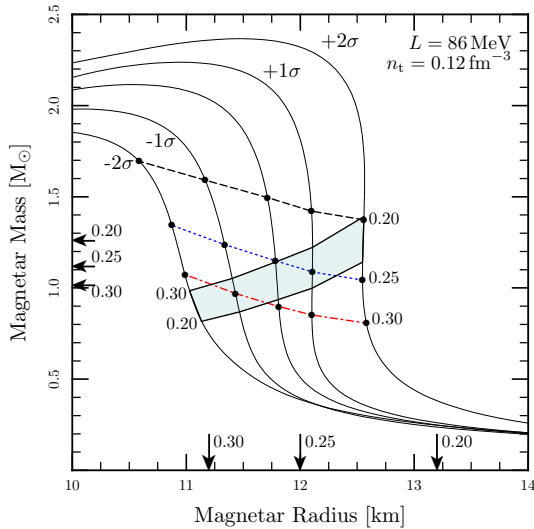


FIG. 7: (Color online) Same as Fig. 6, but for the Rs crust EOS with $B = 0$ G. Here the free neutron entrainment fraction f_{ent} is varied from 0.20 to 0.30, with f_{ent} labeled next to the corresponding curves. The red dot-dashed, blue dotted, and black dashed lines indicate masses and radii from the 29 Hz fundamental mode. The shaded band indicates masses and radii from the 626 Hz harmonic mode. Arrows indicate the masses and radii for $f_{\text{ent}} = 0.30, 0.25,$ and 0.20 that match both the fundamental and harmonic modes.

studied for the equations of state considered here, we assume a fixed fraction of neutron entrainment throughout the entire inner crust. We find that $f_{\text{ent}} \gtrsim 0.75$ is required to have modes consistent with observed QPOs for the SLy4 crust EOS with $L = 46 \text{ MeV}$. For example, with full entrainment, $f_{\text{ent}} = 1.0$, we find $M = 1.35 M_{\odot}$ and $R = 11.9 \text{ km}$. In contrast, for $f_{\text{ent}} = 0.5$ the solution lies outside the $2\text{-}\sigma$ M - R relation from Steiner et al. [17]; extrapolating the fundamental and harmonic curves gives $M = 1.83 M_{\odot}$ and $R = 13.9 \text{ km}$. The Rs crust EOS with $L = 86 \text{ MeV}$ requires $f_{\text{ent}} \lesssim 0.30$ to have modes consistent with observed QPOs. In general, to achieve reasonable values of R with lower values of L requires a larger f_{ent} and a larger n_t .

Although the observed surface dipole field strengths are too weak to affect the fundamental torsional modes of magnetars, the harmonic modes are significantly altered by fields $\gtrsim 10^{15} \text{ G}$. For a transition density at 0.12 fm^{-3} (0.08 fm^{-3}) a magnetic field of $B \gtrsim 4.0 \times 10^{15} \text{ G}$ ($\gtrsim 2.0 \times 10^{15} \text{ G}$) gives no mass and radius solutions consistent at the $2\text{-}\sigma$ level with the mass and radius constraints from PREs and LMXBs. For all crust-core transition densities, a magnetized crust requires a lower mass than the field-free case in order to contain a mode consistent with the observed 626 Hz QPO. The field-free case gives a minimum radius for a crust that can reproduce observations of SGR 1806-20; our model requires $R \geq 11.9 \text{ km}$ for SGR 1806-20. The sensitivity of the harmonic modes to the crust magnetic field strength suggests that the local magnetic field strength cannot greatly exceed the inferred dipole surface field if the QPOs are identified with torsional modes for neutron star masses and radii consistent with those of PREs and LMXBs. We have taken our core EOS models from Steiner et al. [17], who found that smaller radii were disfavored by recent neutron star radius measurements. Recent analysis of quiescent thermal emission from transient neutron stars suggest that the radii are $< 11.1 \text{ km}$ (99%-confidence; Guillot et al. 43). Matching torsional modes to observed QPOs might still be possible in this case if either L or f_{ent} were sufficiently large. This would also require that magnetars have a rather low mass.

Our analysis assumes that the QPOs are due to torsional modes of the crust and that the crust is decoupled from the core. That neutrons in the inner crust would form a superfluid is an idea predating the discovery of neutron stars [44], and there is both theoretical [see, e.g., 45] and observational evidence from cooling transients [46, 47] that the neutrons are below their transition temperature in the inner crust. The neutron superfluid can plausibly decouple the crust and core by eliminating viscous drag [48] and has long been used to explain the long-relaxation times of pulsar glitches [49–51]. In the presence of a magnetic field the crust and core are not completely decoupled. Indeed, Gabler et al. [52] found that for $B \gtrsim 5 \times 10^{13} \text{ G}$ torsional crust modes would be resonantly damped by coupling to the Alfvén continuum, with damping time scales $\sim 0.2 \text{ s}$. Their study did not, however, include the effects of proton pairing in the core nor did it include a realistic model of the neutron star crust. Observations of cooling of the young neutron star in the Cas A supernova remnant [53, 54] suggest that the proton 1S_0 pairing gap is large

[55, 56], so that the protons are in a superconducting state throughout the core. The crust-core coupling depends on the magnetic field configuration and the magnetic field strength near the crust-core interface [20], neither of which are well understood. Understanding the coupling between shear modes and magneto-elastic oscillations in the presence of superfluidity remains challenging. If the threshold field for damping via coupling to the Alfvén continuum were in actuality substantially larger than $B = 5 \times 10^{13}$ G, then the calculations in this paper would still apply.

It is also possible that in the presence of superfluidity, axial perturbations will be pinned to some extent to the core depending on the strength and configuration of the magnetic field. We note that for the magnetic fields studied here ($\leq 2.4 \times 10^{15}$ G), the Alfvén velocity is more than an order of magnitude smaller than the shear velocity at the crust-core interface (see Fig. 2). In this case, magnetic stresses are likely to be much smaller than elastic stresses, and our findings are not likely to change.

Acknowledgments

The authors thank Andrew Cumming and Sanjay Reddy for useful discussions. This work is supported by NASA ATPF grant NNX08AG76G, U.S. DOE grant DE-FG02-00ER41132, Chandra grant TM1-12003X, NSF AST grant 11-09176, and by the Joint Institute for Nuclear Astrophysics at MSU under NSF PHY grant 08-22648.

Appendix A: The Crust Equation of State

To compute the energy density of matter in the crust w , we start with an expression similar to that used by Baym et al. [23]. We take our crust to be composed of “drops” of nuclear matter with volume fraction χ ; within the nucleus the density of neutrons and protons are n_n and n_p , respectively, and we denote $n_l = n_n + n_p$ to be the average baryon density inside a nucleus. The dripped neutrons, with density n_{drip} , occupy a fraction $1 - \chi$ of the volume. The density of nucleons per unit volume is thus $n = \chi(n_n + n_p) + (1 - \chi)n_{\text{drip}}$, and the density of electrons is n_e . As the density approaches nuclear saturation the fraction of space filled by the neutron gas approaches unity.

The energy density w has contributions from nuclei (including the Coulomb lattice contribution), dripped neutrons, and electrons:

$$w(Z, A, n) = \chi \left[n_n m_n + n_p m_p + n_l \frac{E_{\text{bind}}(Z, A)}{A} \right] + (1 - \chi) \epsilon(n_n = n_{\text{drip}}, n_p = 0) + w_e(n_e). \quad (\text{A1})$$

This expression is valid for any baryon density below the transition density ($\approx 10^{14}$ g cm $^{-3}$). Here $\epsilon(n_n, n_p)$ is the energy density, including rest mass, of homogeneous bulk matter at a given neutron and proton number density. We compute ϵ using the bulk matter Hamiltonian in the Skyrme model [57] with SLy4 coefficients [38].

The energy density of the nucleus is

$$n_n m_n + n_p m_p + n_l \frac{E_{\text{bind}}(Z, A)}{A} = \epsilon(n_n, n_p) + \frac{n_l}{A} (E_{\text{surf}} + E_{\text{shell}} + E_{\text{pair}}) + w_{\text{Coul}}. \quad (\text{A2})$$

In this expression, n_n and n_p are the neutron and proton densities inside the nucleus. For the nuclear and lattice contributions to the energy density E_{bind} , we use a liquid-drop mass model [23, 58–60] that includes the lattice contribution in the Coulomb term w_{Coul} , as well as surface (E_{surf}), shell (E_{shell}), and pairing (E_{pair}) corrections to the homogeneous bulk matter Hamiltonian ϵ . At lower densities, the energy per particle in the crust is minimized when $n_{\text{drip}} = 0$, and after the neutron-drip point (about 4×10^{11} g/cm 3), the energy per particle is minimized only when $n_{\text{drip}} > 0$. The baryon number density inside a nucleus n_l is determined from

$$n_l = n_0 + n_2 I^2, \quad (\text{A3})$$

where $I = 1 - 2Z/A$ is the isospin asymmetry, n_0 is the nuclear saturation density of bulk homogeneous matter, and $n_2 < 0$ is a correction due to both the isospin asymmetry, which decreases the saturation density, and the Coulomb interaction, which increases the saturation density [60]. The average neutron and proton densities within the nucleus are then determined from n_l and I via

$$n_n = \frac{n_l}{2}(1 + \eta I), \quad n_p = \frac{n_l}{2}(1 - \eta I), \quad (\text{A4})$$

where $\eta = \delta/I = 0.92$ is a constant of our model that determines the thickness of a neutron skin [60], i.e., the difference between neutron and proton radii, and $\delta = 1 - 2n_p/(n_n + n_p)$ is the density asymmetry.

The next three terms in Equation (A2) are the surface, shell, and pairing corrections. The surface correction is proportional to the surface tension σ , the nuclear surface area $A^{2/3}$, and density asymmetry δ ,

$$E_{\text{surf}} = \sigma \left(\frac{36\pi A^2}{n_l^2} \right)^{1/3} (1 - \sigma_\delta \delta^2) \quad (\text{A5})$$

where $\sigma_\delta > 0$ is a parameter that represents the surface asymmetry [61, 62]. The shell correction to the binding energy per baryon is [27]

$$E_{\text{shell}}(Z, N) = a_1 S_2 + a_2 S_2^2 + a_3 S_3 + a_{np} S_{np}, \quad (\text{A6})$$

where the a_i are fitting parameters,

$$S_2 = \frac{n_v \bar{n}_v}{D_n} + \frac{z_v \bar{z}_v}{D_z}, \quad (\text{A7})$$

$$S_3 = \frac{n_v \bar{n}_v (n_v - \bar{n}_v)}{D_n} + \frac{z_v \bar{z}_v (z_v - \bar{z}_v)}{D_z}, \quad (\text{A8})$$

$$S_{np} = \frac{n_v \bar{n}_v z_v \bar{z}_v}{D_n D_z}, \quad (\text{A9})$$

and

$$\bar{n}_v \equiv D_n - n_v, \quad (\text{A10})$$

$$\bar{z}_v \equiv D_z - z_v. \quad (\text{A11})$$

TABLE II: Parameters of the mass model.

| parameter | SLy4 | Rs |
|-----------------|---------------------------|--------------------------|
| n_0 | 0.1740 fm^{-3} | 0.1597 fm^{-3} |
| n_2 | -0.0157 fm^{-3} | 0.0244 fm^{-3} |
| η | 0.9208 | 0.9043 |
| σ_δ | 1.964 | 1.465 |
| σ | 1.164 MeV | 1.041 MeV |
| a_1 | -1.217 MeV | -1.298 MeV |
| a_2 | 0.0256 MeV | 0.0311 MeV |
| a_3 | 0.00387 MeV | 0.00349 MeV |
| a_{np} | 0.0357 MeV | 0.0287 MeV |
| a_p | 5.277 MeV | 5.265 MeV |

The parameters D_n and D_z correspond to the degeneracy of the neutron and proton shells, i.e., the difference between the magic numbers enclosing the current amount of neutrons or protons. The quantities n_v and z_v are the number of valence neutrons and protons, i.e., the difference between the current number of protons or neutrons and the preceding magic number. The pairing contribution to the nuclear binding energy is taken from Brehm [63] with updated coefficients,

$$E_{\text{pair}} = \begin{cases} -a_p A^{-1/3}, & \text{even-even} \\ +a_p A^{-1/3}, & \text{odd-odd} \\ 0, & \text{even-odd} \end{cases}, \quad (\text{A12})$$

where a_p is a constant of our model. The last term in Equa-

tion (A2) is the Coulomb energy density,

$$w_{\text{Coul.}} = \frac{2\pi}{5} n_p^2 e^2 R_p^2 (2 - 3\chi^{1/3} + \chi), \quad (\text{A13})$$

where e^2 is the Coulomb coupling and R_p is the proton radius ($3Z = 4\pi n_p R_p^3$). The respective χ terms in parentheses correspond to the Coulomb contribution, the lattice contribution, and a correction that accounts for the filling fraction χ of the nuclei. Table II lists the values of the coefficients used in this mass model.

The electronic contribution to the energy density is that of an electron gas embedded in a uniform magnetic field. The electrons acquire an effective mass m_f in the presence of the magnetic field

$$m_f^2 = m_e^2 + 2m_e^2 \left(x + \frac{1}{2} + \frac{1}{2} \nu \right) B_*, \quad (\text{A14})$$

where m_e , x , and ν are respectively the electron mass, principal quantum number, and electron spin along the magnetic field [64, 65]. Here $B_* = \hbar e B / m_e^2 c^3 = B / (4.414 \times 10^{13} \text{ G})$ is the ratio of the magnetic field to the critical field, defined as the field at which the cyclotron energy equals the electron rest-mass. The electron number density and energy density are found by summing over electron states and spins in the limit $\mu_e \gg m_f$.

-
- [1] C. Barat, R. I. Hayles, K. Hurley, M. Niel, G. Vedrenne, U. Desai, V. G. Kurt, V. M. Zhenchenko, and I. V. Estulin, *Astron. & Astrophys.* **126**, 400 (1983).
- [2] G. L. Israel, T. Belloni, L. Stella, Y. Rephaeli, D. E. Gruber, P. Casella, S. Dall'Osso, N. Rea, M. Persic, and R. E. Rothschild, *Astrophys. J. Lett.* **628**, L53 (2005).
- [3] T. E. Strohmayer and A. L. Watts, *Astrophys. J. Lett.* **632**, L111 (2005).
- [4] A. L. Watts and T. E. Strohmayer, *Astrophys. J. Lett.* **637**, L117 (2006).
- [5] R. C. Duncan, *Astrophys. J. Lett.* **498**, L45 (1998).
- [6] A. L. Piro, *Astrophys. J. Lett.* **634**, L153 (2005).
- [7] T. E. Strohmayer and A. L. Watts, *Astrophys. J.* **653**, 593 (2006).
- [8] L. Samuelsson and N. Andersson, *Mon. Not. Royal Astron. Soc.* **374**, 256 (2007).
- [9] A. W. Steiner and A. L. Watts, *Phys. Rev. Lett.* **103**, 181101 (2009).
- [10] H. Sotani, K. Nakazato, K. Iida, and K. Oyamatsu, *Mon. Not. Royal Astron. Soc.* **428**, L21 (2013).
- [11] J. M. Lattimer and M. Prakash, *Phys. Rep.* **442**, 109 (2007).
- [12] A. W. Steiner, *Phys. Rev. C* **85**, 055804 (2012).
- [13] P. Möller, J. R. Nix, W. D. Myers, and W. J. Swiatecki, *At. Data Nucl. Data Tables* **59**, 185 (1995).
- [14] A. Broderick, M. Prakash, and J. M. Lattimer, *Astrophys. J.* **537**, 351 (2000).
- [15] D. Lai and S. L. Shapiro, *Astrophys. J.* **383**, 745 (1991).
- [16] A. W. Steiner, J. M. Lattimer, and E. F. Brown, *Astrophys. J.* **722**, 33 (2010).
- [17] A. W. Steiner, J. M. Lattimer, and E. F. Brown, *Astrophys. J. Lett.* **765**, L5 (2013), 1205.6871.
- [18] K. Glampedakis, L. Samuelsson, and N. Andersson, *Mon. Not. Royal Astron. Soc.* **371**, L74 (2006).
- [19] Y. Levin, *Mon. Not. Royal Astron. Soc.* **368**, L35 (2006).
- [20] M. Gabler, P. Cerdá-Durán, N. Stergioulas, J. A. Font, and E. Müller, *Mon. Not. Royal Astron. Soc.* **421**, 2054 (2012).
- [21] M. van Hoven and Y. Levin, *Mon. Not. Royal Astron. Soc.* **420**, 3035 (2012).
- [22] A. Passamonti and S. K. Lander, *Mon. Not. Royal Astron. Soc.* **429**, 767 (2013).
- [23] G. Baym, H. A. Bethe, and C. J. Pethick, *Nucl. Phys. A* **175**, 225 (1971).
- [24] J. M. Lattimer, C. J. Pethick, D. G. Ravenhall, and D. Q. Lamb, *Nucl. Phys. A* **432**, 646 (1985).
- [25] N. Chamel, R. Pavlov, L. Mihailov, C. Velchev, Z. Stoyanov, et al., *Phys. Rev. C* **86**, 055804 (2012).
- [26] K. Sato, *Progress of Theoretical Physics* **62**, 957 (1979).
- [27] A. E. L. Dieperink and P. van Isacker, *Eur. Phys. Jour. A* **42**, 269 (2009).
- [28] A. K. Harding and D. Lai, *Rep. Prog. Phys.* **69**, 2631 (2006).
- [29] N. Nag, S. Ghosh, and S. Chakrabarty, *Ann. Phys.* **324**, 499 (2009).

- [30] C. Y. Cardall, M. Prakash, and J. M. Lattimer, *Astrophys. J.* **554**, 322 (2001).
- [31] B. L. Schumaker and K. S. Thorne, *Mon. Not. Royal Astron. Soc.* **203**, 457 (1983).
- [32] T. Strohmayer, H. M. van Horn, S. Ogata, H. Iyetomi, and S. Ichimaru, *Astrophys. J.* **375**, 679 (1991).
- [33] R. T. Farouki and S. Hamaguchi, *Phys. Rev. E* **47**, 4330 (1993).
- [34] C. J. Horowitz, A. S. Schneider, and D. K. Berry, *Phys. Rev. Lett.* **104**, 231101 (2010).
- [35] N. Chamel, D. Page, and S. Reddy, *Phys. Rev. C* **87**, 035803 (2013).
- [36] N. Chamel, *Phys. Rev. Lett.* **110**, 011101 (2013).
- [37] J. R. Stone, J. C. Miller, R. Koncewicz, P. D. Stevenson, and M. R. Strayer, *Phys. Rev. C* **68**, 034324 (2003).
- [38] E. Chabanat, P. Bonche, P. Haensel, J. Meyer, and R. Schaeffer, *Phys. Scripta* **T56**, 231 (1995).
- [39] R. Nandi, D. Chatterjee, and D. Bandyopadhyay, *arXiv:1207.3247* (2012).
- [40] K. Oyamatsu and K. Iida, *Phys. Rev. C* **75**, 015801 (2007).
- [41] W. Newton, M. Gearheart, and B.-A. Li, *Astrophys. J. S.* **204**, 9 (2013).
- [42] *McGill SGR/AXP Online Catalog*, <http://www.physics.mcgill.ca/~pulsar/magnetar/main.html>.
- [43] S. Guillot, M. Servillat, N. A. Webb, and R. E. Rutledge, *Astrophys. J.* **772**, 7 (2013).
- [44] A. Migdal, *Nucl. Phys. A* **13**, 655 (1959).
- [45] A. Gezerlis and J. Carlson, *Phys. Rev. C* **81**, 025803 (2010).
- [46] P. S. Shternin, D. G. Yakovlev, P. Haensel, and A. Y. Potekhin, *Mon. Not. Royal Astron. Soc.* **382**, L43 (2007).
- [47] E. F. Brown and A. Cumming, *Astrophys. J.* **698**, 1020 (2009).
- [48] M. A. Ruderman, *Nature (London)* **218**, 1128 (1968).
- [49] G. Baym, C. Pethick, and D. Pines, *Nature* **224**, 673 (1969).
- [50] B. Link, R. I. Epstein, and G. Baym, *Astrophys. J.* **403**, 285 (1993).
- [51] B. Link, *Mon. Not. Royal Astron. Soc.* **422**, 1640 (2012).
- [52] M. Gabler, P. Cerdá Durán, J. A. Font, E. Müller, and N. Stergioulas, *Mon. Not. Royal Astron. Soc.* **410**, L37 (2011).
- [53] C. O. Heinke and W. C. G. Ho, *Astrophys. J. Lett.* **719**, L167 (2010).
- [54] P. S. Shternin, D. G. Yakovlev, C. O. Heinke, W. C. G. Ho, and D. J. Patnaude, *Mon. Not. Royal Astron. Soc. Lett.* **412**, L108 (2011).
- [55] D. Page, M. Prakash, J. M. Lattimer, and A. W. Steiner, *Phys. Rev. Lett.* **106**, 081101 (2011).
- [56] D. G. Yakovlev, W. C. G. Ho, P. S. Shternin, C. O. Heinke, and A. Y. Potekhin, *Mon. Not. Royal Astron. Soc.* **411**, 1977 (2011).
- [57] T. Skyrme, *Nucl. Phys. A* **9**, 615 (1959).
- [58] G. Baym, C. Pethick, and P. Sutherland, *Astrophys. J.* **170**, 299 (1971).
- [59] D. G. Ravenhall, C. J. Pethick, and J. R. Wilson, *Phys. Rev. Lett.* **50**, 2066 (1983).
- [60] A. W. Steiner, *Phys. Rev. C* **77**, 035805 (2008).
- [61] W. D. Myers and W. J. Swiatecki, *Ann. Phys.* **55**, 395 (1969).
- [62] A. W. Steiner, M. Prakash, J. M. Lattimer, and P. J. Ellis, *Phys. Rep.* **411**, 325 (2005).
- [63] J. J. Brehm, *Introduction to the Structure of Matter* (Wiley, 1989).
- [64] I. I. Rabi, *Zeitschrift für Physik* **49**, 507 (1928).
- [65] J. Ventura and A. Potekhin, in *The Neutron Star - Black Hole Connection*, edited by C. Kouveliotou, J. Ventura, and E. van den Heuvel (2001), p. 393.